The Astrophysical Journal Supplement Series, 173:432–440, 2007 December

IR AND UV GALAXIES AT $z = 0.6$: EVOLUTION OF DUST ATTENUATION AND STELLAR MASS AS REVEALED BY SWIRE AND *GALEX*

C. Kevin Xu,[1,2] David Shupe,[3] Veronique Buat,[4] Michael Rowan-Robinson,[5] Thomas Babbedge,[5] Jorge Iglesias-Páramo,[6] Tsutomu T. Takeuchi,[7] Tom A. Barlow,[1] Tim Conrow,[1] Fan Fang,[3] Karl Forster,[1] Peter G. Friedman,[1] Eduardo Gonzales-Solares,[8] Carol Lonsdale,[2] D. Christopher Martin,[1] Patrick Morrissey,[1] Susan G. Neff,[9] David Schiminovich,[1] Mark Seibert,[1] Todd Small,[1] Gene Smith,[10] Jason Surace,[3] and Ted K. Wyder[1]

Received 2006 April 10; accepted 2006 December 4

ABSTRACT

We study dust attenuation and stellar mass of $z \sim 0.6$ star-forming galaxies using new SWIRE observations in IR and *GALEX* observations in UV. Two samples are selected from the SWIRE and *GALEX* source catalogs in the SWIRE/*GALEX* field ELAIS-N1-00 ($\Omega = 0.8$ deg^2). The UV-selected sample has 600 galaxies with photometric redshift (hereafter photo-z) $0.5 \leq z \leq 0.7$ and NUV ≤ 23.5 (corresponding to $L_{\rm FUV} \geq 10^{9.6}\ L_\odot$). The IR-selected sample contains 430 galaxies with $f_{24\ \mu{\rm m}} \geq 0.2$ mJy ($L_{\rm dust} \geq 10^{10.8}\ L_\odot$) in the same photo-$z$ range. It is found that the mean $L_{\rm dust}/L_{\rm FUV}$ ratios of the $z = 0.6$ UV galaxies are consistent with that of their $z = 0$ counterparts of the same $L_{\rm FUV}$. For IR galaxies, the mean $L_{\rm dust}/L_{\rm FUV}$ ratios of the $z = 0.6$ LIRGs ($L_{\rm dust} \sim 10^{11}\ L_\odot$) are about a factor of 2 lower than local LIRGs, whereas $z = 0.6$ ULIRGs ($L_{\rm dust} \sim 10^{12}\ L_\odot$) have the same mean $L_{\rm dust}/L_{\rm FUV}$ ratios as their local counterparts. This is consistent with the hypothesis that the dominant component of LIRG population has changed from large, gas-rich spirals at $z > 0.5$ to major mergers at $z = 0$. The stellar mass of $z = 0.6$ UV galaxies of $L_{\rm FUV} \leq 10^{10.2}\ L_\odot$ is about a factor of 2 less than their local counterparts of the same luminosity, indicating growth of these galaxies. The mass of $z = 0.6$ UV luminous galaxies (UVLGs: $L_{\rm FUV} > 10^{10.2}\ L_\odot$) and IR-selected galaxies, which are nearly exclusively LIRGs and ULIRGs, is the same as their local counterparts.

Subject headings: dust, extinction — galaxies: active — galaxies: evolution — infrared: galaxies — ultraviolet: galaxies

1. INTRODUCTION

The early results from rest-frame UV surveys (Lilly et al. 1996; Madau et al. 1996) reveals an order of magnitude higher star formation rate in $z \sim 1$ galaxies compared to local galaxies. This has been confirmed by recent large-scale UV surveys carried out by *Galaxy Evolution Explorer* (*GALEX*; Martin et al. 2005). The UV luminosity functions for *GALEX* sources at $z \sim 1$ (Arnouts et al. 2005; Schiminovich et al. 2005) and *GALEX* number counts (Xu et al. 2005) are consistent with a luminosity evolution index $\alpha \sim 2.5$ [evolution rate $\propto (1+z)^\alpha$]. The IR/submillimeter surveys reveal a slightly stronger evolution for IR galaxies in the same redshift range, which is also predominantly luminosity evolution with an evolution index in the range of $3 \lesssim \alpha \lesssim 4$ (Blain et al. 1999; Xu 2000; Chary & Elbaz 2001; Le Floćh 2005; Babbedge et al. 2006). In an SDSS study of star formation history of local galaxies ("fossil analysis"), Heavens et al. (2004) concluded that the peak of star formation of the universe is at $z \sim 0.7$. Comparing the luminosity density in the UV (Schiminovich et al. 2005) and that in the FIR (Le Floćh et al. 2005) at different redshifts, the ratio ρ(FIR)/ρ(FUV) increases by about a factor of 4 from $z = 0$ to $z = 1$, indicating a significant evolution in the dust attenuation in star-forming galaxies during this epoch (Takeuchi et al. 2005a).

The most significant obstacle preventing accurate measurements of star formation related quantities is the dust attenuation. The best way to constrain the dust attenuation is through the comparison between the UV and infrared emissions (Xu & Buat 1995; Wang & Heckman 1996; Meurer et al. 1999; Gordon et al. 2000). For local galaxies, the UV/IR comparison has been widely carried out using vacuum UV (100–2000 Å) data and *IRAS* observations (Buat & Xu 1996; Wang & Heckman 1996; Heckman et al. 1998; Iglesias-Páramo et al. 2004). Recent studies using new UV observations obtained in the *GALEX* survey (Martin et al. 2005; Buat et al. 2005; Iglesias-Páramo et al. 2006; Xu et al. 2006) lead to more accurate estimates for the dust attenuation and its dependence on the star formation rate, and the selection effects in the UV and IR samples. There has been limited analysis of the UV/IR comparison of $z > 0.4$ galaxies using *ISO* data and rest-frame near-UV (2800 Å) observations (Flores 1999; Hammer et al. 2005), indicating much higher dust attenuation in these galaxies than that derived from UV-optical SED fits (Hammer et al. 2005). Studies of *Spitzer* observations of COMBO-17 galaxies found no evidence for evolution of the IR-to-UV ratio versus the star formation rate (SFR) relation over the last 7 Gyr (Bell et al. 2005; Zheng et al. 2006).

In this paper, we report a study on UV/IR comparisons for galaxies of photometric redshifts $0.5 \leq z \leq 0.7$. Two samples,

[1] California Institute of Technology, MC 405-47, 1200 East California Boulevard, Pasadena, CA 91125.
[2] Infrared Processing and Analysis Center, California Institute of Technology 100-22, Pasadena, CA 91125.
[3] *Spitzer* Science Center, California Institute of Technology, Mail Stop 220-6, Pasadena, CA 91125.
[4] Observatoire Astronomique Marseille Provence, Laboratoire d'Astrophysique de Marseille, 13012 Marseille, France.
[5] Astrophysics Group, Blackett Laboratory, Imperial College of Science Technology and Medicine, Prince Consort Road, London SW7 2BZ, UK.
[6] Instituto de Astrofisica de Andlucia (CSIC), Camino Bajo de Huetor 50, 18008 Granada, Spain.
[7] Astronomical Institute, Tohoku University, Aoba, Aramaki, Aoba-ku, Sendai 980-8578, Japan.
[8] Institute of Astronomy, Madingley Road, Cambridge CB3 0HA, UK.
[9] Laboratory for Astronomy and Solar Physics, NASA Goddard Space Flight Center, Greenbelt, MD 20771.
[10] Center for Astrophysics and Space Sciences, University of California, San Diego, La Jolla, CA 92093-0424.

one UV-selected and the other IR-selected, are investigated. Galaxies in both samples are star-forming galaxies, with the UV sample including favorably the galaxies with low dust attenuation and the IR sample the galaxies with high dust attenuation (Xu et al. 2006; Buat et al. 2006). We use UV data from the *GALEX* survey and IR data from the *Spitzer* Wide-area Infrared Extragalactic (SWIRE) survey (Lonsdale et al. 2004) to derive the dust attenuation and stellar mass of these galaxies. Comparisons with their local counterparts constrain the evolution of these properties in the UV- and IR-selected galaxies, respectively. In order to take into account the effects due to different selection functions for the $z = 0.6$ samples and $z = 0$ control samples, the comparisons are carried out in luminosity bins where galaxies are found in both the $z = 0.6$ and $z = 0$ samples.

There is a technical consideration for selecting galaxies at $z \sim 0.6$, in addition to the fact that this redshift is close to the peak of cosmic star formation rate found by Heavens et al. (2004): At $z \sim 0.6$, the *GALEX* NUV band (2350 Å) measures the rest-frame FUV band (1530 Å), *Spitzer* IRAC 3.6 μm band is close to rest-frame *K* band (2.2 μm), and the MIPS 24 μm band is close to the rest-frame 15 μm. The rest-frame *K*-band luminosity is the best indicator of stellar mass (Bell et al. 2003), and the rest-frame 15 μm luminosity as an indicator of integrated IR luminosity (5–1000 μm) has been thoroughly investigated in the context of ISOCAM 15 μm observations (Flores et al. 1999; Franceschini et al. 2001; Chary & Elbaz 2001). Therefore, comparisons between $z = 0.6$ galaxies and $z = 0$ galaxies in the corresponding bands will suffer minimum errors due to the *k*-corrections, which can be rather uncertain in the FUV and MIR wave bands.

The paper is organized as following: After this Introduction, the data sets analyzed in this paper are presented in § 2. Major results are listed in § 3. Systematic uncertainties are discussed in § 4. Sections 5 and 6 are devoted to the discussion and conclusion, respectively. Throughout this paper, we assume $\Omega_\Lambda = 0.7$, $\Omega_m = 0.3$, and $H_0 = 70$ km s^{-1} Mpc^{-1}.

2. DATA AND SAMPLE SELECTION

2.1. *GALEX and SWIRE Data*

The data investigated are in the *GALEX* field ELAIS-N1-00, a circular area of 1° diameter centered at R.A. = $16^{\rm h}13^{\rm m}36.8^{\rm s}$ and decl. = $54°59'03.3''$, corresponding to a sky coverage of 0.8 deg^2. The field has been observed by both *GALEX* and SWIRE surveys. The SWIRE 3.6 and 24 μm images and fluxes are taken from "The SWIRE N1 Image Atlases and Source Catalogs" (Surace et al. 2004). The nominal 5 σ sensitivity limit of the SWIRE 24 μm survey is $f_{24} = 0.2$ mJy, but below $f_{24} = 0.25$ mJy the catalog becomes progressively incomplete (Surace et al. 2004; Shupe et al. 2006). The *GALEX* NUV (2350 Å) image, a co-add of observations of 8 orbits with a total $T_{\rm exp} = 7899$ s, is taken from *GALEX* first public data release (*GALEX*-DR1). NUV sources are extracted from the *GALEX* image using IRAF DAOPHOT task. An average foreground extinction of $A_{\rm NUV} = 0.07$ mag, estimated using Schlegel map (Schlegel et al. 1998), has been corrected. Detailed inspections show that the 5 σ detection reaches NUV = 23.5 mag, which is taken as the flux limit of the NUV catalog. Contaminations due to false sources become more severe at magnitudes fainter than this. IR galaxies and UV galaxies undetected either in the optical *r* band (down to $r = 23.5$ mag; Rowan-Robinson et al. 2005) or in the IRAC 3.6 μm band (with the flux limit $f_{3.6\,\mu{\rm m}} = 3.7$ μJy; Surace et al. 2004) are excluded in this analysis. This significantly reduces the number of false sources in both bands. Some extreme populations such as the "extreme 24 μm galaxies" (Yan et al. 2005; Houck et al. 2005), will be missed because of the exclusion of sources without optical counterparts. However, these sources are very rare and most of them are hyperluminous galaxies (HLIRGS) at high redshift ($z \gtrsim 2$; Houck et al. 2005), outside the redshift range of our samples. The selection of sources detected in the IRAC 3.6 μm band should not introduce any significant bias because observations in this band is more than an order of magnitude deeper than that of the NUV and $f_{24\,\mu{\rm m}}$ surveys for an average SED at $z = 0.6$ (see § 5). Galaxies with the UV and/or the IR emission dominated by the active galactic nuclei (AGNs) are not explicitly excluded from this study. It has been shown in the literature that for both the 24 μm–selected samples and the *GALEX*-selected samples, the AGN contamination is insignificant, only about 10%–15% of sources (Franceschini et al. 2005; Bell et al. 2005; Budavari et al. 2005).

2.2. *Photo-z*

The SWIRE photometric redshifts (hereafter photo-*z*) are derived using the template-fitting code I MPZ (Babbedge et al. 2004; Rowan-Robinson 2003). This method considers a set of galaxy and Type 1 AGN templates, along with several priors on dust extinction, stellarity and absolute magnitude with redshift in order to obtain optimal results. It has been extended to incorporate IRAC 3.6 and 4.5 μm data in addition to optical photometry, with the assumption that the emission in the two IRAC short-wavelength bands is dominated by the stellar radiation (Babbedge et al. 2006; Rowan-Robinson et al. 2005). The same "simple stellar populations" (SSPs) templates used in Babbedge et al. (2004), which cover from the UV to the NIR (to $\sim$5 μm), are used. The inclusion of the IRAC 3.6 and 4.5 μm band data has been shown to improve both the reliability and precision of the photo-*z* values (Babbedge et al. 2006; Rowan-Robinson et al. 2005). In particular, the additional NIR data have enabled the rejection of most of the extreme outliers resulting from optical-only results and reduced the dispersion (more details can be found in § 3.1.2 of Babbedge et al. 2006, and in § 5 of Rowan-Robinson et al. 2005). Comparisons to spectroscopic redshifts in ELAIS N1 (I. Pérez-Fournon et al. 2008, in preparation; S. Serjeant et al. 2008, in preparation; Hatziminaoglou et al. 2005) give a total rms scatter, $\sigma_{\rm tot}$, of 0.057 for $(1 + z)$. This is consistent with Rowan-Robinson et al. (2005), who quoted an rms of 6.9% of $(1 + z)$ for ELAIS-N1, where the majority of sources out to redshift $z \sim 0.5$ are galaxies while at higher redshifts (to $z \sim 3$) Type 1 AGNs dominate. The success of the code has also been demonstrated for a number of other fields, filter sets and spectroscopic samples (Babbedge et al. 2006). For all the samples, the mean systematic offset between the photometric and spectroscopic redshifts was found to be essentially zero to the precision of the photometric redshifts. For example, the ELAIS-N1 sample has $\overline{\Delta z}/(1 + z) = 0.0037$.

It should be noted that photometric redshift fitting requires the photometry in each band being measured in the same way. When only using optical data, use of fixed aperture fluxes is sufficient. However, if we include IRAC NIR (3.6 and 4.5 μm) fluxes it is important to be comparing like with like, and these fluxes are integrated fluxes. Hence, for the optical bands, the aperture magnitudes corrected to the integrated magnitudes via curve-of-growth analysis are used. This procedure could introduce errors for galaxies whose integrated SEDs differ largely from the SEDs of their central regions, but in practice the results are consistent, as found in Babbedge et al. (2006).

Another issue is the potential misidentifications between optical sources and IRAC sources due to source confusion, which in turn might affect the accuracy of the photo-*z* results. The accuracy of the cross-IDs of IRAC and optical catalogs of SWIRE

TABLE 1
MEAN IR FLUXES AND IR-TO-UV RATIOS OF $z = 0.6$ UV GALAXIES

$\log L_{\rm FUV}$ ($L_\odot$)	$N_{\rm tot}$	$N_{\rm det}$	$f_{24}^{\rm stack}$ (μJy)	σ (μJy)	$\log (L_{\rm dust}/L_{\rm FUV})$	Error
9.75 ± 0.15	187	21	67	25	0.80	0.17
10.05 ± 0.15	341	68	135	21	0.80	0.12
10.35 ± 0.15	65	24	222	42	0.72	0.13
10.65 ± 0.15	7	5	838	219	0.90	0.14

sources has been discussed extensively in Surace et al. (2004). The flux limits of both the IRAC and optical catalogs are well above the confusion limits (Fazio et al. 2004; J. A. Surace 2006, private communication); therefore, the probability of misidentification due to chance confusion in either band is much less than 1%. Furthermore, the angular resolution of the optical (FWHM $\sim 1''$–$1.5''$) and that of the IRAC 3.6 and 4.5 μm bands (FWHM $\sim 1.6''$) are not very different from each other. Hence, even the genuine close sources (such as galaxy mergers) tend to have the same status as being resolved or confused in both the optical and the IRAC bands in the same time. The effect of the confusion on the photo-z results should be insignificant.

2.3. *Samples*

The *UV sample*, selected in the area considered here and in the photo-z range of $0.5 \leq z \leq 0.7$, has 600 NUV sources brighter than NUV = 23.5 mag. Among them, 117 are detected by *Spitzer* at 24 μm with $f_{24} \geq 0.2$ mJy, corresponding to an IR detection rate of 20%. For *GALEX* sources undetected at 24 μm, upper limits of $f_{24} = 0.2$ mJy are assigned.

The *IR sample* contains 430 SWIRE sources of $f_{24} \geq 0.2$ mJy, selected in the same area and the same photo-z range ($0.5 \leq z \leq 0.7$). Their detection rate by *GALEX* in NUV is 27%. NUV flux upper limits corresponding to NUV = 23.5 mag are assigned to those sources undetected by *GALEX*.

For both UV and IR samples, rest-frame FUV luminosities [νL_ν(1530 Å)] are derived from the NUV (2350 Å) magnitudes and the photo-z. The *Spitzer* 24 μm observations measure the rest-frame 15 μm emission in these $z \sim 0.6$ galaxies, and the total dust luminosity is estimated using the conversion factor $L_{\rm dust} = 11.1 \times L_{15}$ (Chary & Elbaz 2001).

The rest-frame K-band (2.2 μm) luminosity is calculated using $f_{3.6}$ and the photo-z. Stellar mass is estimated from the K-band luminosity using the mass-to-light ratio $M_{\rm stars}/L_{\rm K} = 0.6\ M_\odot/L_\odot$ (Bell et al. 2003), based on a Kroupa IMF (Kroupa et al. 1993). This is about a factor of 2 lower than the mass-to-light ratio derived using the Salpeter IMF (Cole et al. 2001).

Because we are investigating galaxies at a given redshift, the magnitude limit (NUV = 23.5 mag) of the UV-selected sample corresponds to a UV luminosity limit of $L_{\rm FUV} = 10^{9.6}\ L_\odot$ (assuming $z = 0.6$), and the flux limit of the 24 μm–selected sample corresponds to an IR luminosity limit of $L_{\rm dust} = 10^{10.8}\ L_\odot$. Therefore, we are only looking at galaxies in the bright part of the UV and IR luminosity functions. Particularly, for the IR-selected sample, we study nearly exclusively LIRGs ($L_{\rm dust} \geq 10^{11}\ L_\odot$) and ULIRGs ($L_{\rm dust} \geq 10^{12}\ L_\odot$). Given the close to zero mean systematic offset between the photometric and spectroscopic redshifts, our statistical results should be robust against occasional large errors of the photo-z for some individual galaxies ("outliers").

The *control samples* at $z = 0$ are taken from Xu et al. (2006), which are similar to those used in Buat et al. (2005) and Iglesias-Páramo et al. (2006). The UV sample at $z = 0$ includes 94 galaxies brighter than NUV = 16 mag selected from *GALEX* GI1 stage All-sky Imaging Survey (AIS), covering 654 deg^2. The $z = 0$ FIR sample includes 161 galaxies with $f_{60} \geq 0.6$ Jy in 509 deg^2 sky covered both by *GALEX* AIS and *IRAS* PSCz (Saunders et al. 2000). More details can be found in Xu et al. (2006), Buat et al. (2005), and Iglesias-Pátramo et al. (2006). Since many quantities (such as the dust attenuation) have strong luminosity dependence, we always compare the $z = 0.6$ and $z = 0$ galaxies in the same luminosity bins.

3. RESULTS

3.1. *Dust Attenuation in $z = 0.6$ Galaxies*

3.1.1. *UV Galaxies at $z = 0.6$*

The 24 μm detection rate of the $z = 0.6$ NUV sources is only 20% (§ 2). Therefore, for a large majority of these sources the MIR emission is below the SWIRE sensitivity limit. In order to derive meaningful statistics related to the infrared emission, we carried out stacking analysis for galaxies binned into four UV luminosity bins (Table 1).

For each NUV galaxy included in a bin, we cut from the background-subtracted 24 μm mosaic a small subimage, $1'$ on a side, and centered on the coordinates given in the *GALEX* catalog. From a stack of these subimages, we compute a trimmed mean image, excluding 20% of the subimages with the lowest and highest brightness (10% at either end). The purpose of the trimming is to guard against contamination from nearby bright sources, as well as misclassified sources with large photo-z errors ("outliers"). The mean flux density is measured from the trimmed mean image in an aperture of $18''$ diameter. To estimate the standard error of the mean flux density, we use a bootstrap method. From the stack of subimages, we sample with replacement the subimages and make a new trimmed mean image and measure the flux density in the aperture. The resampling is repeated 1000 times, and the sample standard deviation of the aperture measurements provides the uncertainty estimate. The average $\log (L_{\rm dust}/L_{\rm FUV})$ is derived from the mean f_{24}, mean redshift $z = 0.6$, and the mean $L_{\rm dust}$ of the bin. The error of mean $\log (L_{\rm dust}/L_{\rm FUV})$ is the quadratic sum of the error of $f_{\rm NUV}$ and that of $\langle L_{\rm dust} \rangle$. The stacked (trimmed mean) images are shown in Figure 1. The results are reported in Table 1.

In Figure 2 we compare the $L_{\rm dust}/L_{\rm FUV}$ ratios of the $z = 0.6$ UV galaxies with those of the $z = 0$ UV galaxies in the control sample. The FUV attenuation ($A_{\rm FUV}$) values corresponding to given $\log (L_{\rm dust}/L_{\rm FUV})$, marked on the right-hand axis of the plot, are calculated using the following formula taken from Buat et al. (2005):

$$A_{\rm FUV} = -0.00333y^3 + 0.3522y^2 + 1.1960y + 0.4967, \quad (1)$$

where $y = \log (L_{\rm dust}/L_{\rm FUV})$. Small solid squares and arrows represent individual $z = 0.6$ galaxies, and small open diamonds the $z = 0$ galaxies. The arrows, denoting the upper limits in the $z = 0.6$ sample, concentrate in a narrow, tilted region. This is because the redshifts (photo-z) of the galaxies in this sample are in a very narrow range of $0.5 \leq z \leq 0.7$. Therefore, the 25 μm upper limits

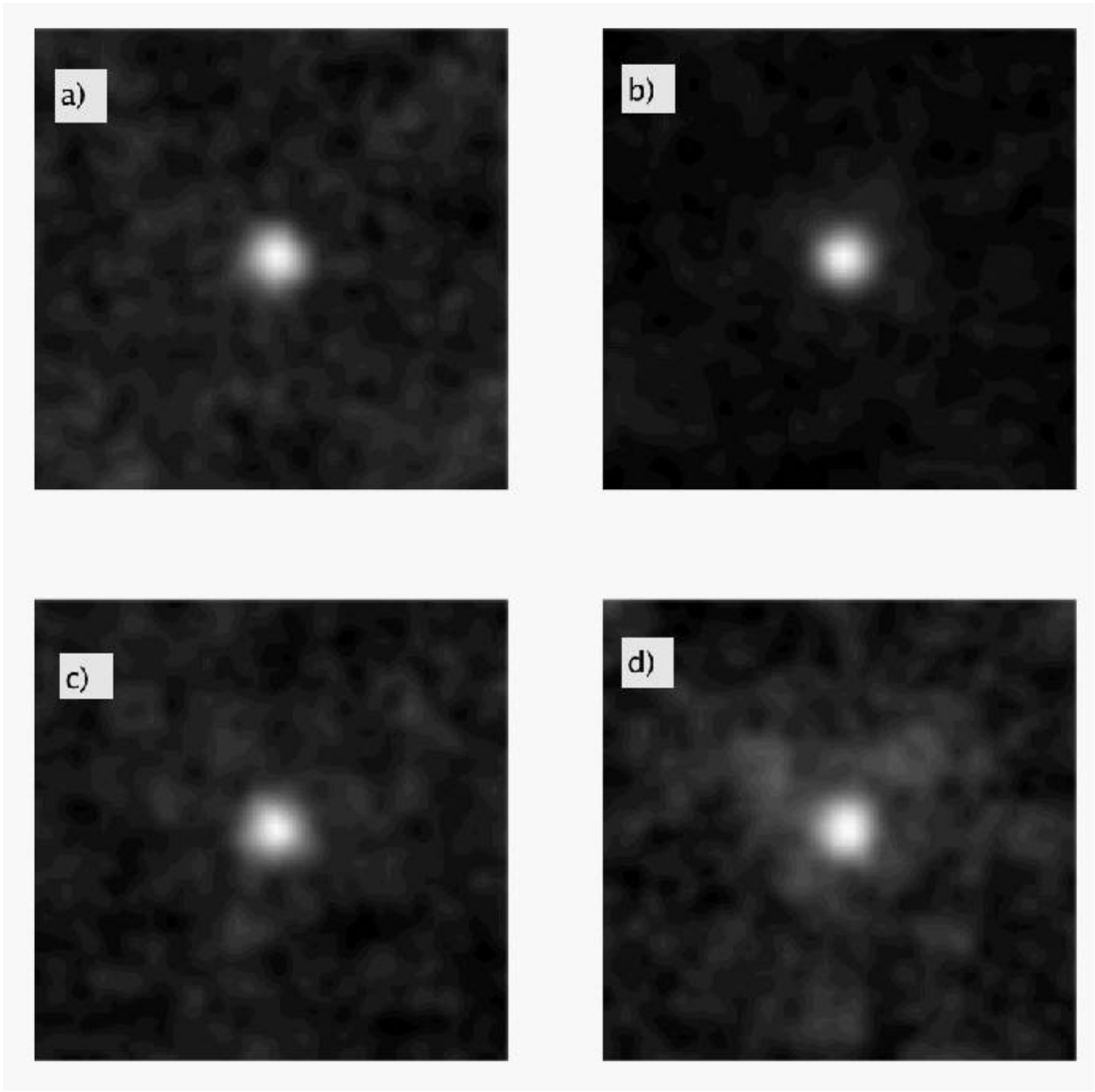

FIG. 1.—Stacked 24 μm images of $z = 0.6$ UV sources in the FUV luminosity bins of (*a*) $9.6 < \log(L_{\rm FUV}/L_{\odot}) \leq 9.9$, (*b*) $9.9 < \log(L_{\rm FUV}/L_{\odot}) \leq 10.2$, (*c*) $10.2 < \log(L_{\rm FUV}/L_{\odot}) \leq 10.5$, and (*d*) $10.5 < \log(L_{\rm FUV}/L_{\odot}) \leq 10.8$.

(0.2 mJy) are translated to a narrow range of $L_{\rm dust}$ upper limits. The large symbols with error bars are the mean ratios in the corresponding luminosity bins. For the $z = 0.6$ sample, they are calculated from the average 25 μm fluxes measured on the stacked images. As demonstrated in Figure 1, good detections are obtained in all four stacked 24 μm images. Therefore, unlike for ratios of individual galaxies, the mean $L_{\rm dust}/L_{\rm FUV}$ ratios are not affected by sensitivity limit of the SWIRE survey. For the $z = 0$ sample, since all individual sources are detected in the IR band, the calculations of the means are straightforward.

For both $z = 0.6$ and $z = 0$ samples, the $L_{\rm dust}/L_{\rm FUV}$ ratio does not show significant dependence on the UV luminosity. It is interesting to note that many $z = 0.6$ UV galaxies with $\log(L_{\rm FUV}) < 10.2$ have $\log(L_{\rm dust}/L_{\rm FUV}) > 1.5$, corresponding to the FUV attenuation $A_{\rm FUV} \gtrsim 3$ mag (Buat et al. 2005), whereas such high dust attenuation is seldom seen in their local counterparts. In the UV luminosity bin of $9.6 \leq \log(L_{\rm FUV}/L_{\odot}) < 9.9$, the mean $L_{\rm dust}/L_{\rm FUV}$ ratios of $z = 0$ and $z = 0.6$ galaxies show a $\sim$80% (i.e., 0.25 dex) difference at $\sim$1 σ level. In the remaining two luminosity bins where the two samples overlap, the mean $L_{\rm dust}/L_{\rm FUV}$ ratios of $z = 0$ and $z = 0.6$ galaxies are very close to each other (difference <50%). Recently, Burgarella et al. (2006) found evidence for about half of $z \sim 1$ UV bright galaxies to have very low dust attenuation ($A_{\rm FUV} \sim 0.5$–0.6 mag). We did not detect the same trend for $z \sim 0.6$ UV galaxies.

3.1.2. *IR Galaxies at* $z = 0.6$

For the 430 $z = 0.6$ galaxies in the 24 μm–selected sample, the detection rate in the *GALEX* NUV band is also low (27%). Therefore, the stacking analysis is again exploited in deriving the mean NUV fluxes. Galaxies are binned into four IR luminosity bins (Table 2). Because the depth of the NUV image is very close to the confusion limit (NUV = 24 mag, Xu et al. 2005), we choose to subtract sources brighter than NUV = 23.5 mag (5 σ detections) from the image before stacking. In principle this approach should yield a cleaner result (Zheng et al. 2006) than simply stacking all sources because the contamination due to bright neighboring sources outside the sample (i.e., sources of different redshifts) is minimized. Again, we derive the trimmed mean of the NUV flux for each bin of IR-selected galaxies by excluding 20% of galaxies with the highest and the lowest measured NUV fluxes (10% on each side) and estimate the errors by bootstrapping (1000

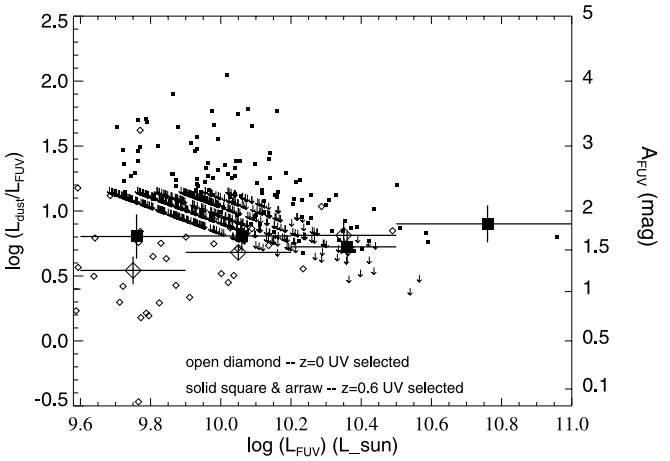

FIG. 2.—Plot of $\log (L_{\rm dust}/L_{\rm FUV})$ vs. $\log (L_{\rm FUV})$ for the UV-selected samples at $z = 0.6$ and $z = 0$. Arrows denote upper limits. Large solid squares with error bars represent the means for $z = 0.6$ galaxies, derived through stacking analysis. Large open diamonds with error bars represent the means for $z = 0$ galaxies. The right-hand axis of the plot marks the FUV attenuation ($A_{\rm FUV}$) corresponding to the $\log (L_{\rm dust}/L_{\rm FUV})$.

replicate simulations). For each $L_{\rm dust}$ bin, the average $\log L_{\rm dust}/L_{\rm FUV}$ and its error are derived in the same way as for UV galaxies in a given $L_{\rm FUV}$ bin. The results are reported in Table 2.

In Figure 3 we compare the $L_{\rm dust}/L_{\rm FUV}$ ratios of the $z = 0.6$ IR galaxies with those of their $z = 0$ counterparts. Same as in Figure 2, small symbols and arrows represent individual galaxies, and large symbols with error bars the means in corresponding luminosity bins. In contrast with the UV galaxies in Figure 2, both $z = 0.6$ and $z = 0$ IR galaxies show strong dependence of the $L_{\rm dust}/L_{\rm FUV}$ ratio with the luminosity. In the luminosity range covered by the $z = 0.6$ sample ($\gtrsim 10^{11}\ L_\odot$), the $L_{\rm dust}/L_{\rm FUV}$ ratios of IR galaxies are 1–2 orders of magnitude higher than those of the UV galaxies (Fig. 2). It appears that $z = 0.6$ IR galaxies have a steeper slope in the $\log (L_{\rm dust}/L_{\rm FUV})$ versus $\log (L_{\rm dust})$ relation than $z = 0$ IR galaxies. The mean $L_{\rm dust}/L_{\rm FUV}$ of $z = 0.6$ galaxies in the bin $10.8 \leq \log (L_{\rm dust}/L_\odot) < 11.2$ is significantly lower, by a factor of $\sim$2.5, than that of their local counterparts, indicating that $z = 0.6$ LIRGs [$\log (L_{\rm dust}/L_\odot) \sim 11$] have lower dust attenuation compared to their local counterparts. On the other hand, as shown in Figure 3, $z = 0.6$ ULIRGs [$\log (L_{\rm dust}/L_\odot) \sim 12$] have similar dust attenuation as local ULIRGs.

Bell et al. (2005) and Zheng et al. (2006), in their studies of MIPS observations of COMBO-17 galaxies, concluded that there is no evolution in the $L_{\rm dust}/L_{\rm FUV}$ versus SFR relation over the last 7 Gyr. It is not straightforward to compare their results with ours because our sample is IR-selected, whereas COMBO-17 is an optical sample. The analysis of Bell et al. (2005) is based on a comparison of the $L_{\rm dust}/L_{\rm FUV}$ versus SFR plot of individual $z \sim 0.7$ galaxies with that of their local counterparts (Fig. 1 of Bell et al. 2005), which can be affected by the presence of large fraction ($\sim$70%) of upper limits in the MIPS data. In Figure 9 of Zheng et al. (2006), only galaxies in the top two panels (corresponding to the $M_{\rm B}$ bins of $[M_* - 1,\ M_*]$ and $[M_*,\ M_* + 1]$) include LIRGs (SFR $> 10\ M_\odot\ {\rm yr}^{-1}$). For these galaxies, there is indeed a trend that, while the average SFR increases by about an order of magnitude from $z = 0.15$ to $z = 0.95$, the $L_{\rm dust}/L_{\rm FUV}$ ratio increases very little, at least significantly less than what is predicted by the $L_{\rm dust}/L_{\rm FUV}$ versus SFR relation. Le Floc'h et al. (2005) studied a MIPS-selected sample (median redshift $\sim$0.7) among COMBO-17 galaxies. Inspections of their $L_{\rm IR}/L_{\rm UV}$ versus LIR plot (their Fig. 10*c*) show that the median $L_{\rm IR}/L_{\rm UV}$ of the LIRGs in that sample is also significantly lower than that of local LIRGs, consistent with our result.

3.2. *Stellar Mass of $z = 0.6$ Galaxies*

3.2.1. *UV Galaxies at $z = 0.6$*

The stellar mass of $z = 0.6$ galaxies is estimated using the IRAC 3.6 μm flux, which measures the rest-frame K-band emission (§ 2.2). For the control samples at $z = 0$, the stellar mass is estimated using the total magnitude ($m_{\rm tot}$) of the 2MASS K_s (2.16 μm) band (Jarrett et al. 2000).

Interestingly, as shown in Figure 4, the stellar mass of $z = 0.6$ UV galaxies fainter than $L_{\rm FUV} = 10^{10.2}\ L_\odot$ is on average a factor of 1.5–2 lower than that of their local counterparts. This result is statistically significant at the 2 σ level. These galaxies are in the category of "intermediate massive galaxies" ($3 \times 10^{10}\ M_\odot \leq M \leq 3 \times 10^{11}\ M_\odot$) as defined by Hammer et al. (2005). According to Heavens et al. (2004), the star formation in these galaxies peaked at $z \sim 0.6$. Hammer et al. (2005) argued that the mass of these galaxies increased by about a factor of 2 since $z = 1$. Our result is consistent with this. On the other hand, the $z = 0.6$ UV luminous galaxies (UVLGs; Heckman et al. 2005) of $L_{\rm FUV} > 10^{10.2}\ L_\odot$ have the same mean stellar mass as their local counterparts.

3.2.2. *IR Galaxies at $z = 0.6$*

In Figure 5 we compare the stellar mass of $z = 0.6$ IR galaxies with that of their local counterparts. Here, unlike for UV galaxies, no systematic difference is found between the means of $z = 0.6$ and $z = 0$ galaxies. Both samples show the same trend that more luminous galaxies have higher stellar mass.

It should be pointed out that for bright IR galaxies, particularly the ULIRGs, the contribution from the violent starburst to the rest-frame NIR emission can be significant (Surace et al. 2000), accounting for up to $\sim$50% of the *K*-band flux. Therefore the stellar mass estimated using the rest-frame *K* band should be treated with caution. On the other hand, the conclusion derived from Figure 5 should not be affected by this if the contamination from the starburst is the same for the $z = 0$ and for the $z = 0.6$ galaxies of the same luminosity.

TABLE 2
MEAN UV FLUXES AND IR-TO-UV RATIOS OF $z = 0.6$ IR GALAXIES

$\log (L_{\rm dust})$ ($L_\odot$)	$N_{\rm tot}$	$N_{\rm det}$	$\rm NUV^{stack}$ (mag)	σ (mag)	$\log (L_{\rm dust}/L_{\rm FUV})$	Error
11.0 ± 0.2	172	52	24.15	0.20	1.37	0.11
11.35 ± 0.15	200	50	24.30	0.18	1.74	0.11
11.65 ± 0.15	49	12	24.22	0.28	2.04	0.12
12.0 ± 0.2	9	3	23.76	0.39	2.25	0.16

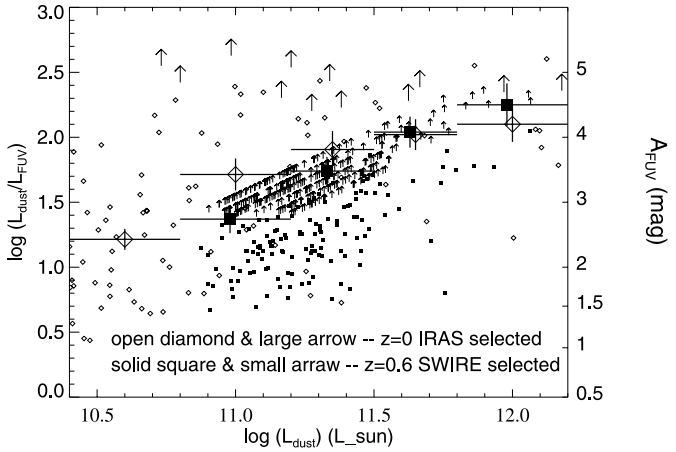

FIG. 3.—Plot of L_{dust}/L_{FUV} vs. L_{dust} for the IR-selected samples at $z = 0.6$ and $z = 0$. Arrows denote upper limits. The large solid squares with error bars represent the means for $z = 0.6$ galaxies. The large open diamonds with error bars represent the means for $z = 0$ galaxies.

3.2.3. *Comparison between UV and IR Galaxies*

UV and IR samples select low and high dust attenuation galaxies, respectively (Xu et al. 2006; Buat et al. 2006). Given the dependence of the dust attenuation on stellar mass (Wang & Heckman 1996; Burgarella et al. 2005), the UV galaxies tend to have lower stellar mass than the IR galaxies. This is indeed what we see in Figures 4 and 5. In particular, no IR galaxy in the $z = 0.6$ sample has the stellar mass less than $10^{10.3}\,M_{\odot}$, while as many as about 20% of galaxies in the $z = 0.6$ UV sample have stellar mass below this. It should be noted that the IRAC 3.6 μm band flux limit $f_{3.6\,\mu m} = 3.7$ μJy corresponds to a stellar mass limit of $M = 10^{9.4}\,M_{\odot}$, a factor of $\sim$2 ($\sim$8) lower than the minimum stellar mass of the $z = 0.6$ UV galaxies (IR galaxies). This demonstrates again that very few (if any) galaxies might have been missed by our UV and IR samples due to the IRAC 3.6 μm flux limit.

UVLGs in the last two UV luminosity bins in Figure 4 have their mean $L_{dust} > 10^{11}\,L_{\odot}$ (Table 1), therefore belonging to the LIRG population as well. These are galaxies with the most active star formation in the universe, likely being in the peak phase of some brief (and perhaps recurrent) starburst episodes (Hammer et al. 2005). In the literature, three mechanisms have been considered for the triggering of starbursts, including (1) major merger, (2) minor merger, and (3) bar instability during the secular evolution of disk galaxies (Hammer et al. 2005; Bell et al. 2005; Combes 2006). There is some indication that relative importance of these mechanisms has changed since $z \sim 1$ (Melbourne et al. 2005). Our results in Figures 4 and 5 indicate that, no matter which mechanism dominates the triggering of LIRG/ULIRG activity, the host galaxies of these starburst events in the $z = 0.6$ and $z = 0$ universe have the same stellar mass.

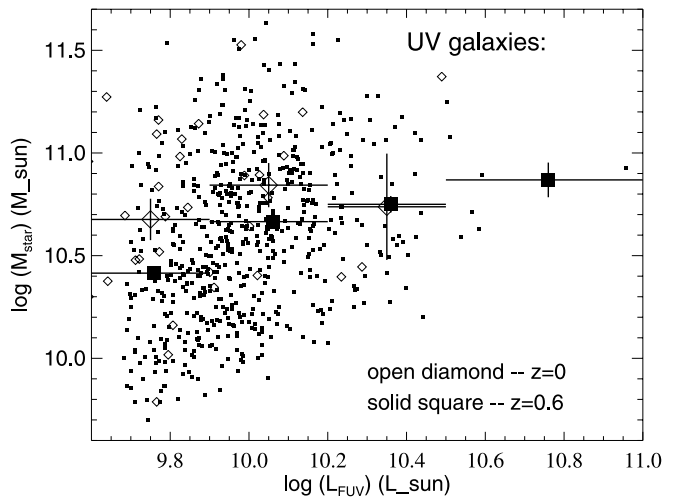

FIG. 4.—Plot of stellar mass (estimated using rest-frame K-band luminosity) vs. FUV luminosity for UV-selected samples at $z = 0.6$ (*solid squares*) and $z = 0$ (*open diamonds*). The small symbols represent individual galaxies, whereas the large symbols with error bars denote the corresponding means.

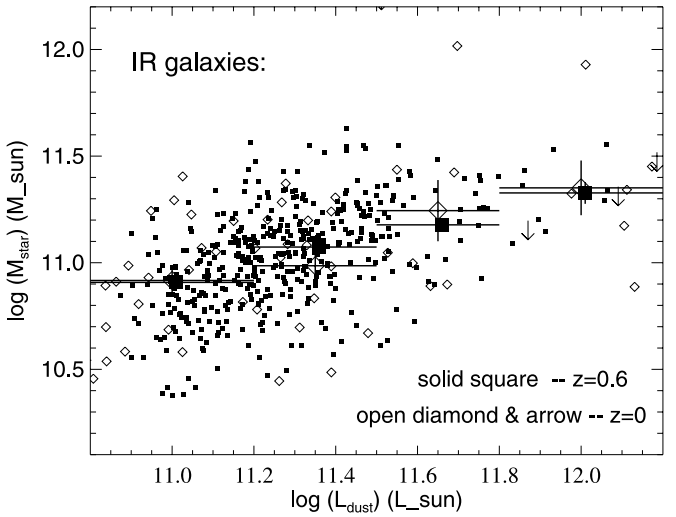

FIG. 5.—Plot of stellar mass vs. L_{dust} for IR-selected samples at $z = 0.6$ (*solid squares*) and $z = 0$ (*open diamonds*). The small symbols represent individual galaxies, whereas the large symbols with error bars denote the corresponding means.

4. SYSTEMATIC UNCERTAINTIES

4.1. *The L_{dust}/L_{15} Ratio*

The most important source of systematic uncertainty in this work is due to the extrapolation from L_{15} to L_{dust}. The analysis of SEDs local IR galaxies by Chary & Elbaz (2001) has shown that $L_{dust} \propto L_{15}^{0.998\pm0.021}$, therefore the L_{dust}/L_{15} ratio has little dependence on the luminosity (see also Takeuchi et al. 2005b). We checked this result using the IR SEDs of a larger sample of 831 *IRAS* galaxies that are constructed "semiempirically" by Xu et al. (2001). The result is plotted in Figure 6. Xu et al. (2001) divided the SED sample into 3 subclasses according to the *IRAS* colors: normal disk galaxies ($f_{60}/f_{25} > 5$ and $f_{100}/f_{60} \geq 2$), starburst galaxies ($f_{60}/f_{25} > 5$ and $f_{100}/f_{60} < 2$), and AGNs ($f_{60}/f_{25} \leq 5$). As shown in Figure 6, indeed for normal disks and starbursts the L_{dust}/L_{15} ratio is rather constant against the luminosity. The mean L_{dust}/L_{15} of normal disk galaxies is 11.5 ± 3.1 and that of starburst galaxies is 11.0 ± 2.8, both very close to the value of Chary & Elbaz (2001), which is 11.1. On the other hand, there is a significant trend for galaxies with AGNs in the sense that the ratio decreases with L_{15}. The mean of IR galaxies with AGNs is 4.9 ± 3.8, about a factor of 2 lower than those of normal disk and starburst galaxies. Therefore, we might have significantly overestimated the L_{dust} if galaxies in any of the luminosity bins studied here are dominated by AGNs. In Figure 6, the ratios of two famous ULIRGs, Arp 220 (29.5) and Mrk 231 (5.9), the former a prototype of "cold ULIRGs," which are mostly starbursts, and the latter a prototype of "warm ULIRGs" mostly AGNs, are also plotted as references. In addition to the intrinsic variations in the L_{dust}/L_{15} ratio, the effect of possible SED evolution in $z = 0.6$ galaxies has to be taken into account, too.

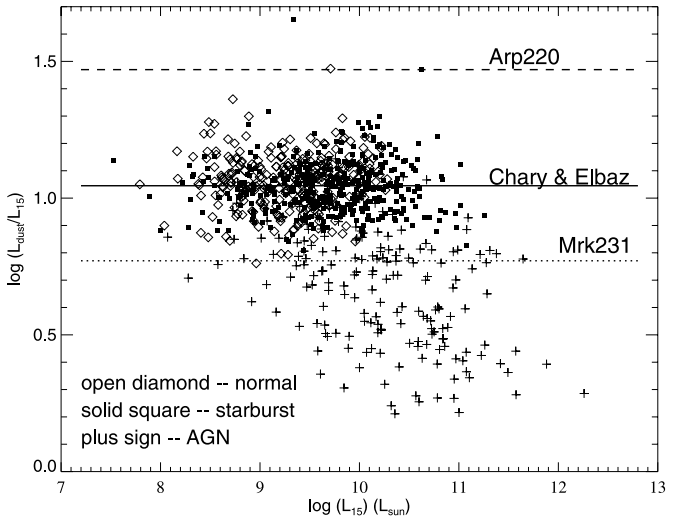

FIG. 6.—Plot of $L_{\rm dust}/L_{15}$ vs. L_{15} for local IR galaxies in the SED library of Xu et al. (2001).

The most direct way to constrain this uncertainty is to look at the real SEDs of the $z = 0.6$ galaxies detected in longer wavelength bands of *Spitzer*, in particular the MIPS 160 μm (rest-frame 100 μm) band. However, it turned out that only 1 source in the $z = 0.6$ IR sample is detected at 160 μm above the nominal 5 σ sensitivity limit of $f_{160} = 100$ mJy (Surace et al. 2004). A much more robust method is to stack the 70 and 160 μm images of the galaxies in a given luminosity bin and use the mean f_{70}/f_{24} and f_{160}/f_{24} derived from the stacked images to constrain the mean SED. The 70 and 160 μm images are taken from the same SWIRE database. For each luminosity bin, SEDs taken from the sample plotted in Figure 6 are selected according to the IR luminosity range, the mean f_{70}/f_{24} and f_{160}/f_{24} and their uncertainties (including 20% calibration uncertainty). The mean $L_{\rm dust}/L_{15}$ ratio and the uncertainty are derived using these SEDs. The results are given in Tables 3 and 4 and plotted in Figure 7. Note that for UV galaxies in the luminosity bin of $9.6 \leq \log(L_{\rm FUV}/L_\odot) < 9.9$, no detections are found even on the stacked 70 and 160 μm images, therefore only upper limits are listed. For galaxies in other luminosity bins in both Tables 3 and 4, the detections on stacked 70 and 160 μm images are significant (>3 times of the noise), although some of the errors of the mean flux ratios (particularly those of f_{160}/f_{24}) are as high as 90%. In these cases the error of the mean is largely due to the statistical dispersion of the variable.

For all UV-selected galaxies, the derived mean $L_{\rm dust}/L_{15}$ ratios for all 4 luminosity bins are consistent with that of Chary & Elbaz (2001). For IR-selected galaxies, only the mean ratio of galaxies in the brightest bin of $11.8 \leq \log L_{\rm dust} < 12.2$ is significantly below the calibration of Chary & Elbaz (2001). As shown in Figure 8, the SED that fits the mean FIR colors of the bin is much closer to that of Mrk 231 than Arp 220, suggesting that many galaxies in this bin have their 24 μm flux enhanced by AGN dust torus emission. This can be compared with the *ISO* results (Genzel et al. 1998), which show that most of the *IRAS* 60 μm band selected $z = 0$ ULIRGs of $L_{\rm dust} \sim 10^{12}\ L_\odot$ are powered by starbursts, and AGN contribution is important only for ULIRGs with $L_{\rm dust} > 2 \times 10^{12}\ L_\odot$ (Veilleux et al. 1998). The increased contribution in the MIR of AGNs in the ULIRGs of our $z = 0.6$ IR sample is at least partly a consequence of the MIR (rest-frame 15 μm) selection. Whether this also indicates a difference between $z = 0$ and $z = 0.6$ ULIRGs requires further investigation. Meanwhile, as shown in Figure 3, if the mean $L_{\rm dust}$ of the $z = 0.6$ galaxies in the last luminosity bin is reduced by a factor of 2, their $L_{\rm dust}/L_{\rm FUV}$ ratio is still consistent with that of the local ULIRGs.

4.2. *Source Confusion*

The angular resolutions of the MIPS 24 μm maps and *GALEX* NUV maps are very well matched, both having FWHM $\sim 6''$. The astrometry of *GALEX* sources is accurate to $\sim 1''$ (Seibert et al. 2005), and that of SWIRE sources is even better (Surace et al. 2004). This ensures minimal mismatches between sources in the two bands. The contamination from nearby foreground bright sources is insignificant in the measurement of the 24 μm fluxes of the NUV sources. According to published 24 μm number counts (Papovich et al. 2004; Shupe et al. 2006), the chance for a random source of $f_{24} > 0.2$ mJy to fall into the beam of an NUV source is less than 1%. For the measurement of the NUV fluxes of 24 μm sources, the chance of this contamination is higher (at $\sim$2% level according to the NUV counts of Xu et al. 2005). In order to minimize it, we did the stacking of the NUV images after subtracting sources brighter than NUV = 23.5 mag (§ 3.1). Our choice of using the "trimmed mean" to estimate the average fluxes in the luminosity bins should exclude sources seriously affected by bright neighbors. The confusion due to fainter sources adds another noise (confusion noise) to the total error budget. It could bias the measured flux of a stacked image to higher value only if the source population is strongly clustered (Takeuchi & Ishii 2004). For the NUV and 24 μm sources, this is not the case. Heinis et al. (2004) found that UV galaxies are only very weakly clustered. For the 24 μm sources, as shown by Zheng et al. (2006), the confusion noise behaves very close to the random Gaussian noise down to very faint flux level ($\sim$0.3–0.4 μJy). Uncorrelated confused sources add an uniform diffuse background on the image, which is subtracted in the normal background subtraction task during the flux measurement. In summary, uncertainties due to source confusion are unlikely to introduce significant bias to our results.

5. DISCUSSION

5.1. *Difference between $z = 0.6$ and $z = 0$ LIRGs*

In their study of faint galaxies in GOODS-N field, Melbourne et al. (2005) concluded that there is strong evidence for a

TABLE 3
MEAN FIR COLORS AND $L_{\rm dust}/L_{15}$ RATIOS OF $z = 0.6$ UV GALAXIES

$L_{\rm FUV}$ ($L_\odot$)	f_{70}/f_{24}	Error	f_{160}/f_{24}	Error	$L_{\rm dust}/L_{15}$	Error
9.75 ± 0.15	<11.4	...	<24.4	...	<12.0	...
10.05 ± 0.15	6.1	3.0	27.8	20.2	11.5	2.2
10.35 ± 0.15	10.3	4.7	38.9	25.0	11.9	2.4
10.65 ± 0.15	4.1	3.0	19.3	14.2	9.6	2.2

TABLE 4
MEAN FIR COLORS AND $L_{\rm dust}/L_{15}$ RATIOS OF $z = 0.6$ IR GALAXIES

$L_{\rm FUV}$ ($L_\odot$)	f_{70}/f_{24}	Error	f_{160}/f_{24}	Error	$L_{\rm dust}/L_{15}$	Error
11.0 ± 0.2	3.9	2.0	15.0	13.8	8.7	2.1
11.35 ± 0.15	4.7	1.5	21.2	8.4	9.1	1.6
11.65 ± 0.15	6.5	1.8	31.7	13.2	11.5	2.2
12.0 ± 0.2	4.4	2.3	8.5	8.1	5.0	2.1

morphological evolution of the populations of LIRGs since redshift $z = 1$. They found that above $z = 0.5$, roughly half of all LIRGs are spirals and the peculiar/irregular-to-spiral ratio is $\sim$0.7, whereas at low z, spirals count for only one-third of LIRGs and the peculiar/irregular-to-spiral ratio is 1.3. Similarly, Bell et al. (2005) found that at $z \sim 0.7$, the IR luminosity density for $10.7 \lesssim \log(L_{\rm IR}/L_\odot) \lesssim 11.5$ is dominated by spiral galaxies, and the contribution from clearly interacting galaxies with morphology suggestive of major mergers is at most 30%. Our result of the significantly lower mean $L_{\rm dust}/L_{\rm FUV}$ ratios (i.e., dust attenuation) for the $z = 0.6$ LIRGs compared to those of their local counterparts, is in line with these findings. As shown in local samples (Sanders & Mirabel 1996), noninteracting LIRGs usually are large, gas-rich spirals with widely distributed star formation all over the disk. In contrast, most of major-merger LIRGs have their star formation concentrates in the nuclei. These nuclear starbursts are highly compact, and they generally show very high dust attenuation (and warmer IR colors). If indeed the composite of LIRGs has changed from spiral dominant at $z \sim 0.6$ to major-merger dominant at $z = 0$, the increase of the mean dust attenuation for these galaxies since $z = 0.6$, as revealed in this work, is expected. On the other hand, even at high z, the population of ULIRGs is still dominated by major mergers (Bell et al. 2005). This provides a simple explanation of why the difference between the mean $L_{\rm dust}/L_{\rm FUV}$ ratios of $z = 0.6$ and $z = 0$ galaxies does not extend to higher luminosity bins in Figure 3.

5.2. *Evolution of Cosmic Dust Attenuation*

There has been strong evidence for a positive (backward) evolution of the mean dust attenuation in star-forming galaxies of $z \lesssim 1$ (Takeuchi et al. 2005a). From the *GALEX* deep survey of VVDS field, Schiminovich et al. (2005) derived an evolution rate for the UV luminosity density up to $z = 1$ in the form of $\rho_{1500\,\text{Å}} \propto (1+z)^{2.5\pm0.7}$; at the same time, Le Floćh et al. (2005) found from the *Spitzer* MIPS 24 μm deep survey of the CDFS field that the IR luminosity function evolves between $0 \le z \le 1$ as $L^*_{\rm IR} \propto (1+z)^{3.2^{+0.7}_{-0.2}}$ and $\phi^*_{\rm IR} \propto (1+z)^{0.7^{+0.2}_{-0.6}}$, corresponding to an IR luminosity density evolution of $\rho_{\rm IR} \propto (1+z)^{3.9}$. Therefore, the ratio between the IR and UV luminosity densities increases by a factor of $(1+0.6)^{1.4} = 1.9$ from $z = 0$ to $z = 0.6$, indicating a significant increase of cosmic dust attenuation during this redshift interval.

Interestingly, in this work, it is found that for galaxies of given UV or IR luminosities the dust attenuation did not increase with the redshift. Actually, there is evidence that the dust attenuation in $z = 0.6$ LIRGs is even *lower* than that in the local LIRGs. Is this consistent with the positive backward evolution of cosmic dust attenuation? The key to understanding the apparent contradiction lies in the strong dependence of the dust attenuation on the SFR (Buat & Burgarella 1998; Heckman et al. 1998; Martin et al. 2005; Xu et al. 2006) and in the fact that SFR of the "average" star-forming galaxy at $z = 0.6$ is much higher than the "average" star-forming galaxy at $z = 0$. It is worthwhile to check out whether this interpretation works quantitatively. Assume the SFR of the average star-forming galaxy evolving as $(1+z)^3$, which is consistent with luminosity evolution of both UV and IR galaxies. Then take the local ($z = 0$) $L_{\rm dust}/L_{\rm FUV}$ versus SFR relation, which can be approximated by a linear dependence $L_{\rm dust}/L_{\rm FUV} \propto$ SFR above SFR $\sim 0.1\,M_\odot\,{\rm yr}^{-1}$ (Xu et al. 2006). Accordingly, from $z = 0$ to $z = 0.6$, the average $L_{\rm dust}/L_{\rm FUV}$ ratio should increase by a factor of $(1+0.6)^3 = 4.1$, about a factor of 2 more than what is observed. Hence, it appears that combining the cosmic SFR evolution with local $L_{\rm dust}/L_{\rm FUV}$ versus SFR relation predicts *too much* evolution of cosmic dust attenuation. This again suggests that the major population of star-forming galaxies at $z = 0.6$, of which contribution from LIRGs can be significant

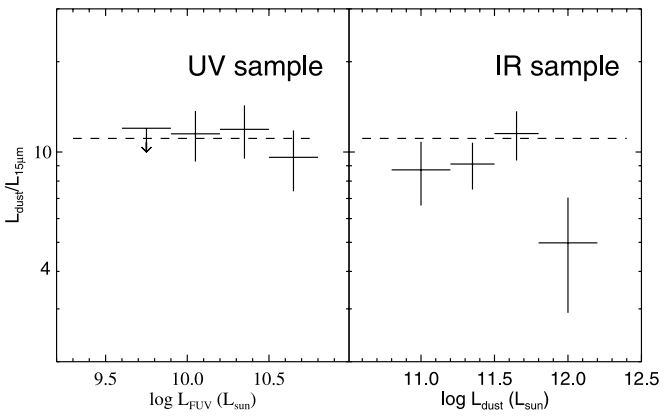

FIG. 7.—Mean $L_{\rm dust}/L_{15}$ ratios for $z = 0.6$ UV galaxies (*left panel*) and for $z = 0.6$ IR galaxies (*right panel*), estimated using the mean f_{160}/f_{24} and f_{70}/f_{24} ratios derived by stacking. The dotted line specifies the adopted standard taken from Chary & Elbaz (2001).

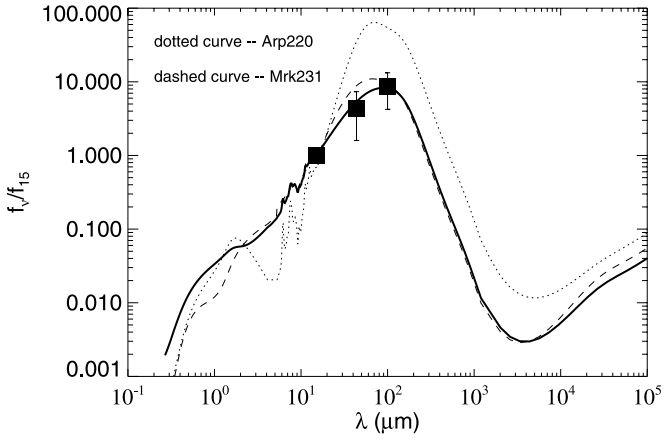

FIG. 8.—Plot of the rest-frame SED (*solid curve*) that fits the mean FIR color ratios (*solid squares with error bars*) of $z = 0.6$ ULIRGs [IR galaxies of $11.8 \le \log(L_{\rm dust}/L_\odot) < 12.2$]. Compared to the SED of Arp 220 (*dotted curve*) and that of Mrk 231 (*dashed curve*).

(Hammer et al. 2005; Bell et al. 2005), may have less dust attenuation than that of $z = 0$ galaxies of the same SFR.

6. CONCLUSION

Using new SWIRE observations in the IR and *GALEX* observations in the UV, we study the dust attenuation and stellar mass of two samples of $z \sim 0.6$ galaxies in the SWIRE/*GALEX* field ELAIS-N1-00 ($\Omega = 0.8$ deg^2). The first sample is UV-selected, having 600 galaxies with photometric redshift $0.5 \leq z \leq 0.7$ and NUV ≤ 23.5 mag (corresponding to $L_{\rm FUV} \geq 10^{9.6}\ L_\odot$ for $z = 0.6$). The second sample is IR-selected, containing 430 galaxies with $f_{24\,\mu{\rm m}} \geq 0.2$ mJy ($L_{\rm dust} \geq 10^{10.8}\ L_\odot$ at $z = 0.6$) and in the same photometric redshift range. The $L_{\rm dust}$ is derived from the rest-frame 15 μm luminosity. The dust attenuation is estimated using the luminosity ratio $L_{\rm dust}/L_{\rm FUV}$. Because of the low 24 μm detection rate (20%) of the UV galaxies and the low UV detection rate (27%) of the IR galaxies, the stacking technique is exploited in deriving mean $L_{\rm dust}/L_{\rm FUV}$ ratios in given $L_{\rm FUV}$ and $L_{\rm dust}$ bins for UV- and IR-selected samples, respectively. The stellar mass is derived using the SWIRE 3.6 μm flux, which measures the rest-frame K-band 2.2 μm emission. These results are compared to $L_{\rm dust}/L_{\rm FUV}$ ratios and the stellar mass of galaxies in control samples at $z = 0$. It is found that the mean $L_{\rm dust}/L_{\rm FUV}$ ratios of the $z = 0.6$ UV galaxies are consistent with that of their $z = 0$ counterparts of the same $L_{\rm FUV}$. For IR galaxies, the mean $L_{\rm dust}/L_{\rm FUV}$ ratios of the $z = 0.6$ LIRGs are about a factor of 2 lower than local LIRGs, whereas $z = 0.6$ ULIRGs have the same mean $L_{\rm dust}/L_{\rm FUV}$ ratios as their local counterparts. This is consistent with results in the literature that show evidence of population changes of LIRGs from major-merger dominant at $z = 0$ to spiral dominant at $z > 0.5$. The stellar mass of $z = 0.6$ UV galaxies of $L_{\rm FUV} \leq 10^{10.2}\ L_\odot$ is about a factor of 2 less than their local counterparts of the same luminosity, indicating growth of these galaxies. The mass of $z = 0.6$ UVLGs ($L_{\rm FUV} > 10^{10.2}\ L_\odot$) and IR-selected galaxies, which are nearly exclusively LIRGs and ULIRGs, is the same as their local counterparts.

GALEX (*Galaxy Evolution Explorer*) is a NASA Small Explorer, launched in 2003 April. We gratefully acknowledge NASA's support for construction, operation, and science analysis for the *GALEX* mission, developed in cooperation with the Centre National d'Etudes Spatiales of France and the Korean Ministry of Science and Technology. Support for this work, part of the *Spitzer Space Telescope* Legacy Science Program, was provided by NASA through an award issued by JPL under NASA contract 1407. This publication makes use of data products from the Two Micron All Sky Survey, which is a joint project of the University of Massachusetts and the Infrared Processing and Analysis Center/California Institute of Technology, funded by NASA and NSF.

REFERENCES

Arnouts, S., et al. 2005, ApJ, 619, L43
Bell, E. F., McIntosh, D. H., Katz, N., & Weinberg, M. D. 2003, ApJS, 149, 289
Bell, E. F., et al. 2005, ApJ, 625, 23
Babbedge, T., et al. 2006, MNRAS, 370, 1159
———. 2004, MNRAS, 353, 654
Blain, A. W., Smail, I., Ivison, R. J., & Kneib, J.-P. 1999, MNRAS, 302, 632
Budavari, T., et al. 2005, ApJ, 619, L31
Buat, V., & Burgarella, D. 1998, A&A, 334, 772
Buat, V., & Xu, C. 1996, A&A, 306, 61
Buat, V., et al. 2005, ApJ, 619, L51
———. 2006, ApJS, 173, 404
Burgarella, D., et al. 2006, A&A, 450, 69
Burgarella, D., Buat, V., & Iglesias-Páramo, J. 2005, MNRAS, 360, 1413
Chary, R. R., & Elbaz, D. 2001, ApJ, 556, 562
Cole, S., et al. 2001, MNRAS, 326, 255
Combes, F. 2006, in IAU Symp. 235, Galaxy Evolution across the Hubble Time, ed. F. Combes & J. Palous (Cambridge: Cambridge Univ. Press), 19
Fazio, G. G. 2004, ApJS, 154, 39
Flores, H., et al. 1999, A&A, 343, 389
Franceschini, A., Aussel, H., Cesarsky, C. J., Elbaz, D., & Fadda, D. 2001, A&A, 378, 1
Franceschini, A., et al. 2005, AJ, 129, 2074
Genzel, R., et al. 1998, ApJ, 498, 579
Gordon, K., Clayton, G. C., Witt, A. N., & Misselt, K. A. 2000, ApJ, 533, 236
Hammer, F., et al. 2005, A&A, 430, 115
Hatziminaoglou, E., et al. 2005, AJ, 129, 1198
Heavens, A., Benjamin, P., Jimenez, R. & Dunlop, J. 2004, Nature, 428, 625
Heckman, T. M., Robert, C., Leitherer, C., Garnett, D. R., & van der Rydt, F. 1998, ApJ, 503, 646
Heckman, T. M., et al. 2005, ApJ, 619, L35
Heinis, S., et al. 2004, A&A, 424, L9
Houck, J. R., et al. 2005, ApJ, 622, L105
Iglesias-Páramo, J., Buat, V., Donas, J., Boselli, A., & Milliard, B. 2004, A&A, 419, 109
Iglesias-Páramo, J., et al. 2006, ApJS, 164, 38
Jarrett, T., et al. 2000, AJ, 119, 2498
Kroupa, P., Tout, C. A., & Gilmore, G. 1993, MNRAS, 262, 545
Le Floćh, E., et al. 2005, ApJ, 632, 169
Lilly, S. J., Le Févre, O., Hammer, F., & Crampton, D. 1996, ApJ, 460, L1
Lonsdale, C., et al. 2004, ApJS, 154, 54. 2005, ApJ, 632, 169
Madau, P., et al. 1996, MNRAS, 283, 1388
Martin, D. C., et al. 2005, ApJ, 619, L59
Melbourne, J., Koo, D. C., & Le Floćh, E. 2005, ApJ, 632, L65
Meurer, G. R., Heckman, T. M., & Calzetti, D. 1999, ApJ, 521, 64
Papovich, C., et al. 2004, ApJS, 154, 70
Rowan-Robinson, M. 2003, MNRAS, 345, 819
Rowan-Robinson, M., et al. 2005, AJ, 129, 1183
Sanders, D. B., & Mirabel, I. F. 1996, ARA&A, 34, 749
Saunders, W., et al. 2000, MNRAS, 317, 55
Schiminovich, D., et al. 2005, ApJ, 619, L47
Schlegel, D. J., Finkbeiner, D. P., & Davis, M. 1998, ApJ, 500, 525
Seibert, M., et al. 2005, ApJ, 619, L23
Shupe, D. L., et al. 2006, AJ, submitted
Surace, J. A., Sanders, D. B., & Evans, A. S. 2000, ApJ, 529, 170
Surace, J. A., et al. 2004, SWIRE ELAIS N1 Source Catalogs, (Pasadena: SSC)
Takeuchi, T. T., Buat, V., & Burgarella, D. 2005a, A&A, 440, L17
Takeuchi, T. T., Buat, V., Iglesias-Páramo, J., & Burgarella, D. 2005b, A&A, 432, 423
Takeuchi, T. T., & Ishii, T. T. 2004, ApJ, 604, 40
Veilleux, S., Sanders, D. B., & Kim, D.-C. 1998, ApJ, 522, 139
Wang, B., & Heckman, T. M. 1996, ApJ, 457, 645
Xu, C. 2000, ApJ, 541, 134
Xu, C., & Buat, V. 1995, A&A, 293, L65
Xu, C., Lonsdale, C. J., Shupe, D. L., O'Linger, J., & Masci, F. 2001, ApJ, 562, 179
Xu C. K., et al. 2006, ApJ, 646, 834
———. 2005, ApJ, 619, L11
Yan, L., et al. 2005, ApJ, 628, 604
Zheng, X. Z., et al. 2006, ApJ, 640, 784